Supplementary Information

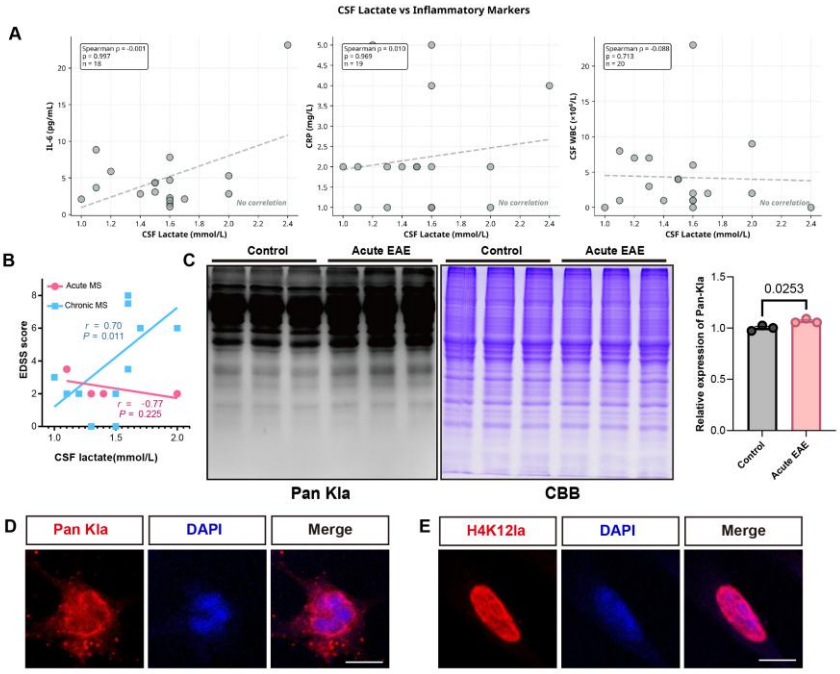

Supplementary Fig. 1 Correlation Analysis and Subcellular Localization of Protein Lactylation.

(A) Correlation analysis between CSF lactate levels and inflammatory markers (IL-6, CRP, and CSF WBC) in MS patients. Spearman correlation coefficients () and p-values are shown.(B) Correlation between CSF lactate and EDSS scores in MS patients stratified by disease phase. Spearman correlation (ρ) shows a significant positive association in chronic MS ($\rho = 0.61$, $P = 0.012$).(C) Western blot of global lysine lactylation (Pan Kla) in spinal cord tissues from control and acute EAE mice. Coomassie Brilliant Blue (CBB) staining of the gel was used as the loading control for total protein normalization. The bar graph shows the densitometric quantification of total Pan Kla signals normalized to the total protein density. Data are mean ± SEM (n = 3 biological replicates per group). Statistical significance was determined using the unpaired two-tailed Student's t-test (*$p < 0.05$).(D) Subcellular localization of total protein lactylation (Pan Kla). Confocal imaging shows signals in both the cytoplasm and nucleus.(E) Subcellular localization of H4K12la. Signals are strictly confined to the DAPI-positive nuclei. Scale bars in (D, E), 10 μm.

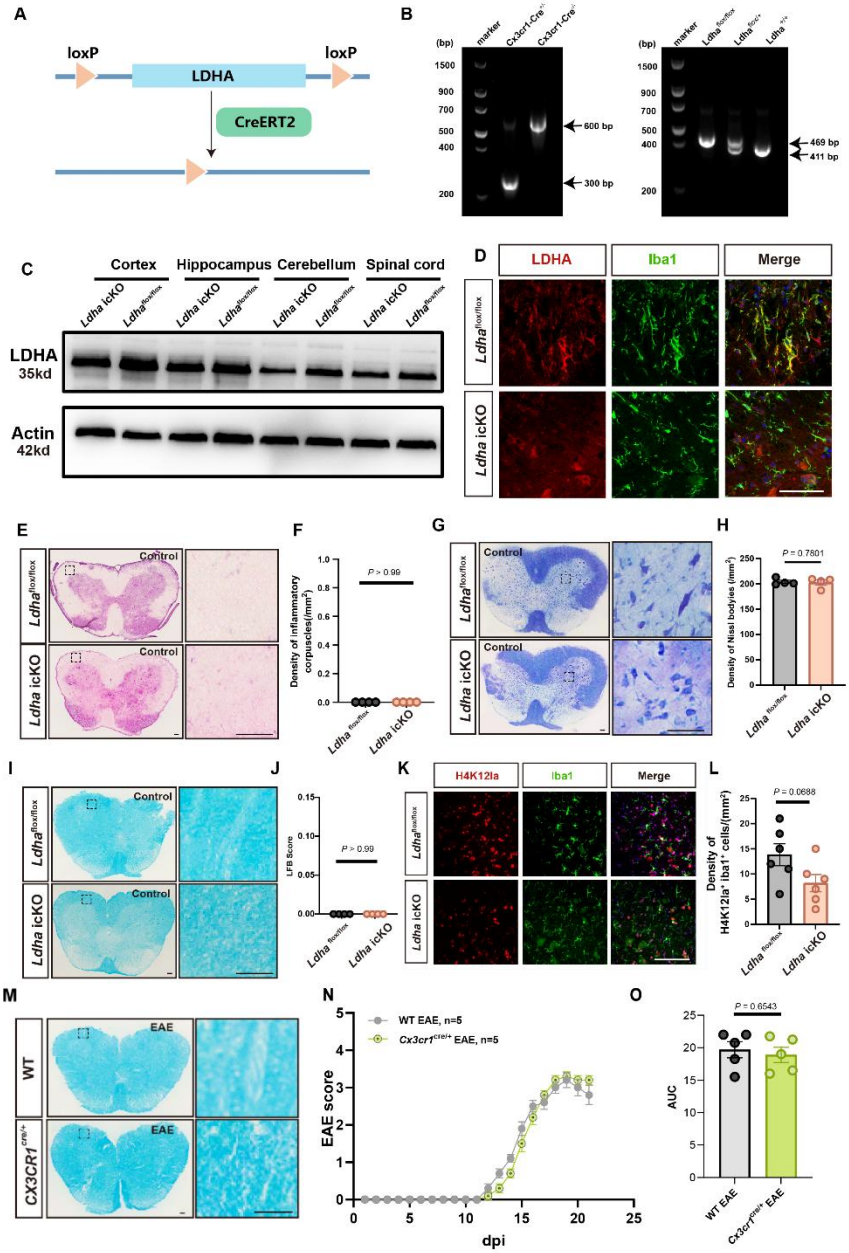

Supplementary Fig. 2 Characterization of microglial Ldha icKO mice and control validations.
(A, B) Breeding strategy for generating inducible microglial-specific Ldha knockout mice (A) and genotyping results for the *Cx3cr1*-CreERT2 and *Ldha* alleles (B). (C) Western blot analysis of LDHA protein expression across different CNS regions in tamoxifen-treated control and Ldha icKO mice. Actin serves as a loading control. (D) Representative immunofluorescence images of LDHA (red) and Iba1 (green) in the spinal cord. (E-J) Representative H&E (E), Nissl (G), and LFB (I) staining with corresponding quantifications of inflammatory cell density (F), neuronal density (H), and myelin scores (J) in healthy control and Ldha icKO

spinal cords (n = 5 mice per group). (K,L) Representative immunofluorescence (K) and quantification (L) of H4K12la^{+} Iba1^{+} cell density in healthy control and Ldha icKO mice (n = 6 mice per group). (M-O) Representative LFB staining (M), clinical EAE scores (N), and AUC quantification (O) in wild-type and *Cx3cr1*$^{CreERT2/+}$ control mice (n = 5 mice per group). Scale bars, 50 µm (applies to all other image panels). Data are presented as mean ± SEM. Statistical significance was determined by an unpaired, two-tailed Student's t-test. Exact P values: (h) P = 0.7801; (l) P = 0.0688; (o) P = 0.6543.

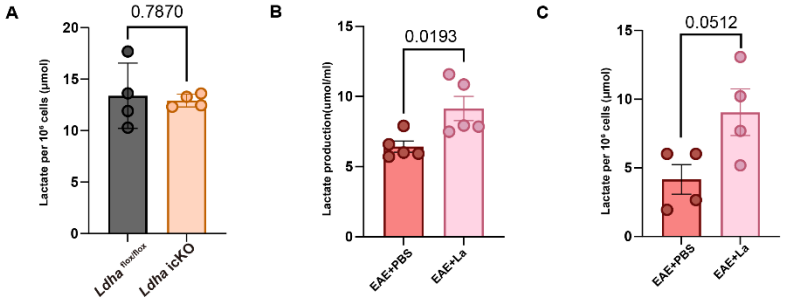

Supplementary Fig. 3 Verification of lactate penetration and conditional knockout specificity. (A) L-lactate production in peripheral splenic CD11b+ myeloid cells isolated from *Ldha*$^{flox/flox}$ controls and Ldha icKO mice. (n = 4 mice per group) (B-C) L-lactate concentrations in spinal cord tissue (B) (n = 5 mice per group) and isolated CD11b+ cells (C) (n = 4 mice per group) following systemic administration in EAE mice. Data represent mean ± SEM. Statistical significance was determined by an unpaired, two-tailed Student's t-test. Exact P values: (A) P = 0.7870; (B) P = 0.0193; (C) P = 0.0512.

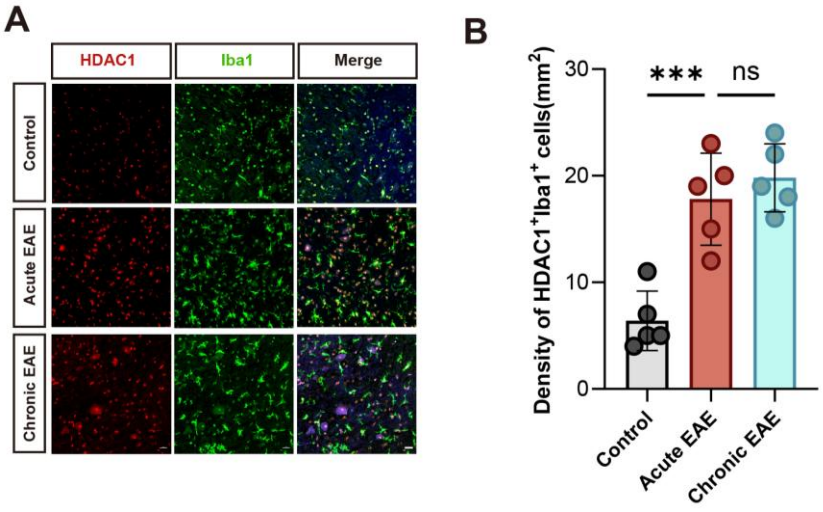

Supplementary Fig. 4 Baseline regulation of HDAC1 in microglial cells during EAE progression. (A) Representative immunofluorescence images of HDAC1 (red) and Iba1 (green) in spinal cord tissues from Control, Acute EAE, and Chronic EAE mice. DAPI (blue) stains nuclei. Scale bars, 50 µm (applies to all image panels).(B) Quantification of HDAC1^{+} Iba1^{+} cell density (n = 5 mice per group). Data are presented as mean ± SEM. Statistical significance was determined by a one-way ANOVA followed by Tukey's multiple comparisons test. Exact P values: ANOVA F(2, 12) = 21.36, P = 0.0001; Tukey's post hoc: Control vs. Acute EAE adjusted P = 0.0006, Acute EAE vs. Chronic EAE adjusted P = 0.6488.

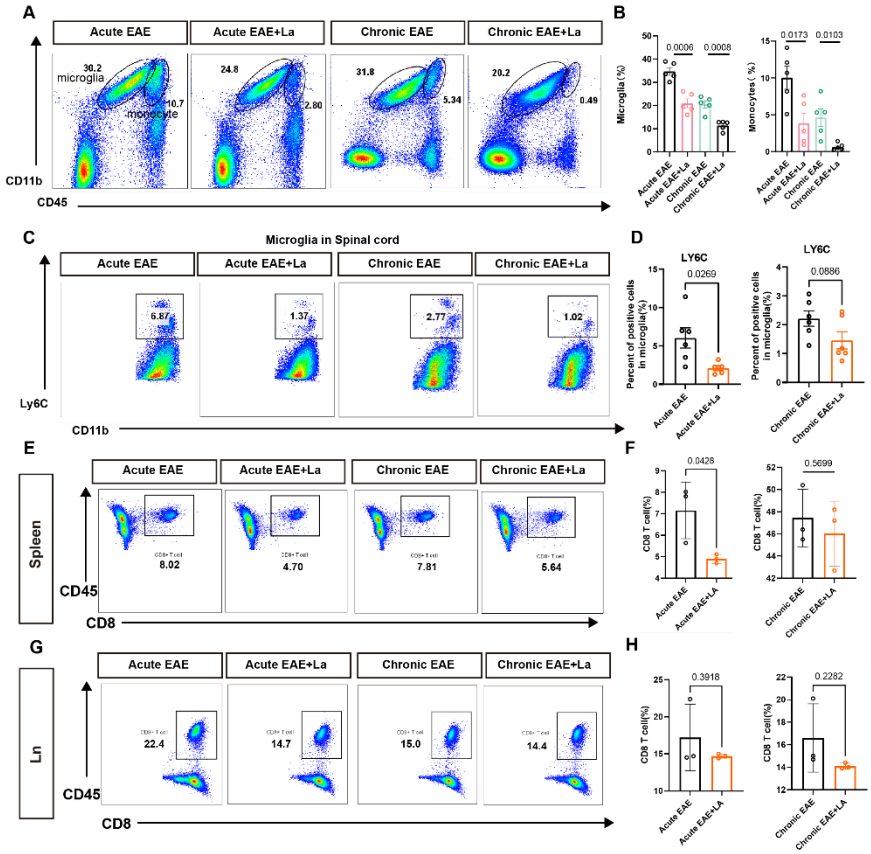

Supplementary Fig. 5 Lactate Treatment Modulates CNS and Peripheral Immune Cell Populations during EAE.

(A, B) Representative flow cytometry plots (A) and quantification (B) of microglia (CD45intCD11b^{+}) and infiltrating monocytes (CD45^{hi}CD11b^{+}) in the spinal cord of EAE mice at acute and chronic phases with or without lactate treatment (n = 5 mice per group).(C, D) Representative flow cytometry plots (C) and quantification (D) of CD8^{+} T cells in the spleen of EAE mice at acute and chronic phases (n = 3 mice per group).(E, F) Representative flow cytometry plots (E) and quantification (F) of CD8^{+} T cells in the draining lymph nodes (Ln) of EAE mice at acute and chronic phases (n = 3 mice per group).Data are presented as mean ± SEM. Statistical significance was determined by an unpaired, two-tailed Student's t-test. Source data are provided as a Source Data file.

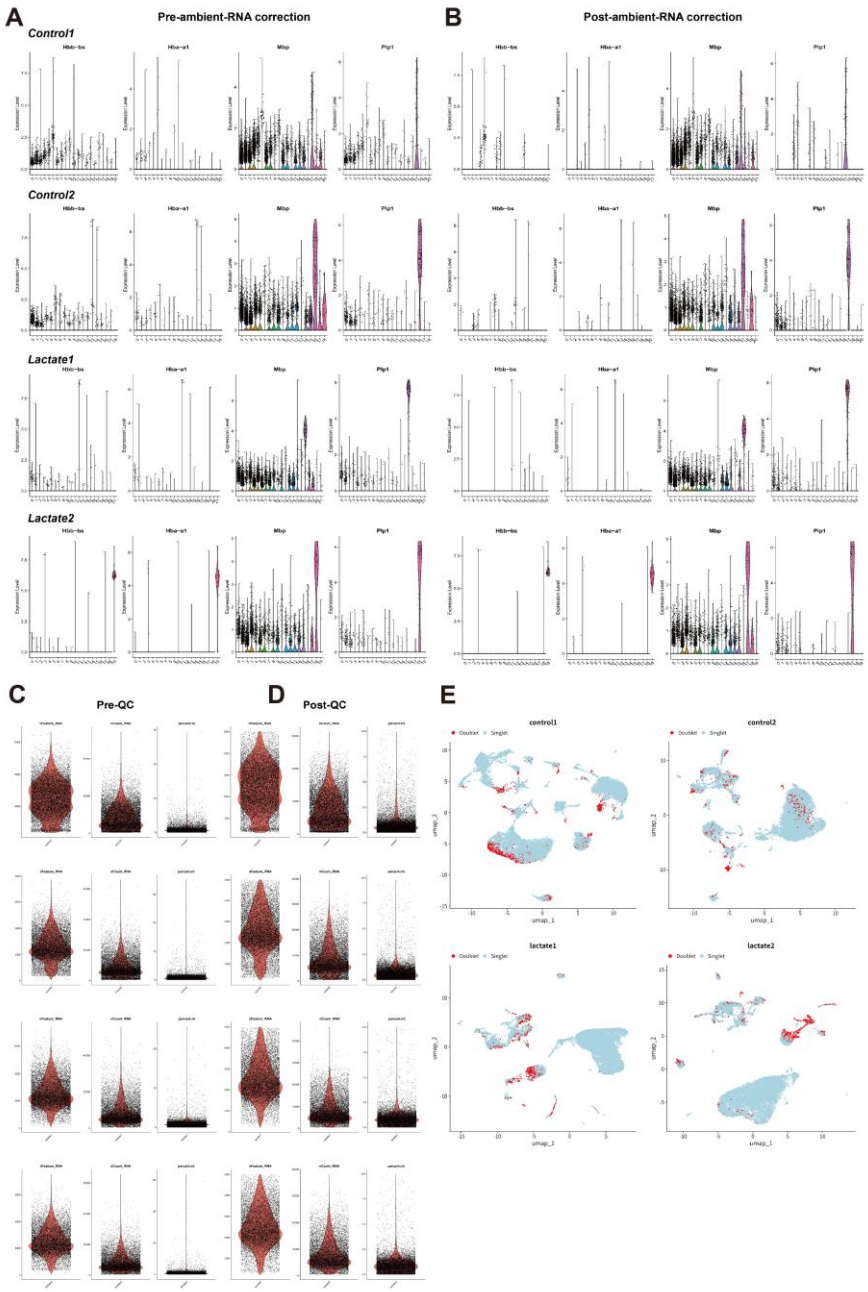

Supplementary Fig. 6 Rigorous quality control pipeline and data preprocessing.
(A-B) Evaluation and correction of ambient RNA contamination. Violin plots show the expression levels of hemoglobin genes (*Hbb-bs, Hba-a1*) and myelin genes (*Mbp, Plp1*) in each cluster before (A) and after (B) correction using SoupX. Note the effective removal of background noise in non-relevant clusters.(C-D)

Distribution of key quality control metrics—number of detected genes (nFeature_RNA), unique molecular identifier counts (nCount_RNA), and percentage of mitochondrial genes (percent.mt)—before (C) and after (D) applying stringent filtering criteria.(E) Identification and removal of doublets. UMAP plots visualize the distribution of singlets (blue) and doublets (red) identified by DoubletFinder in each sample, which were subsequently excluded from downstream analysis.

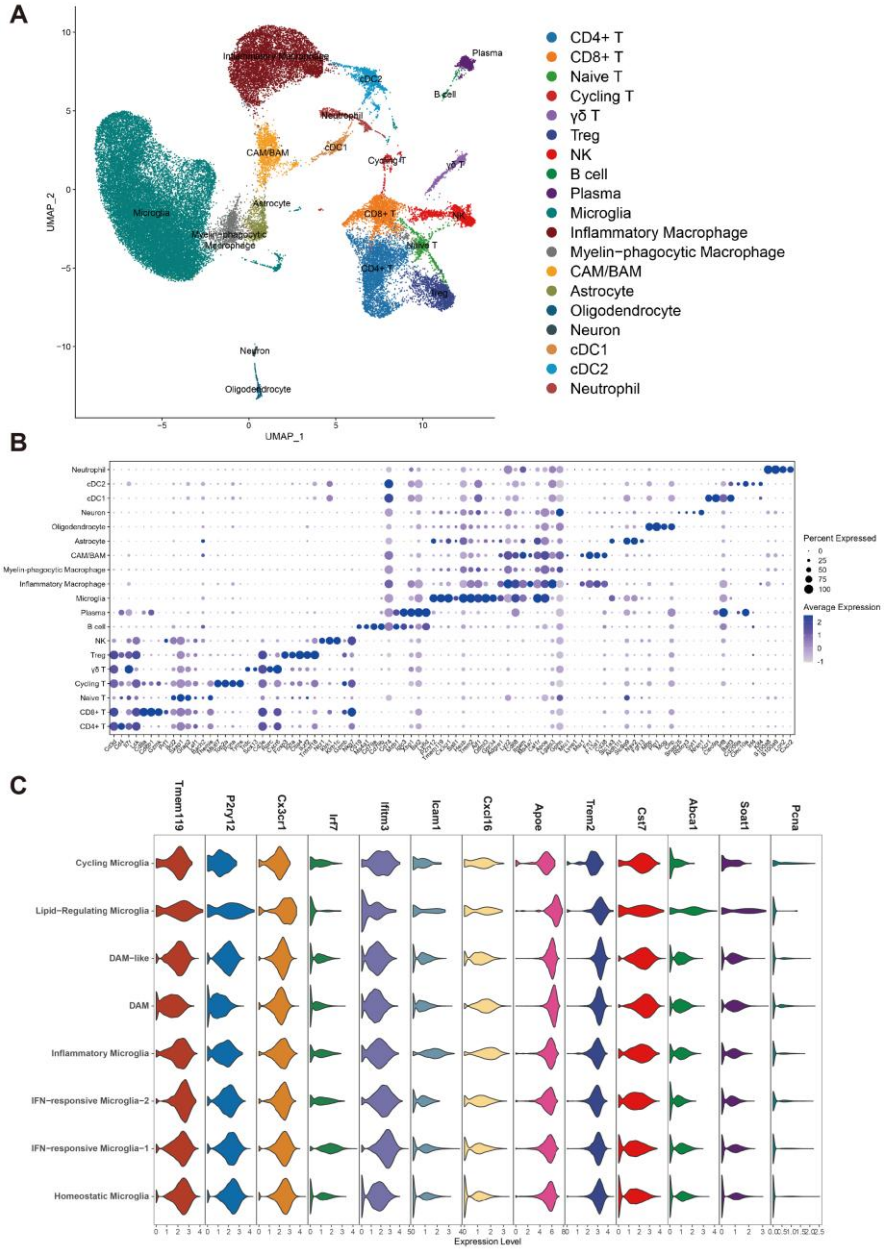

Supplementary Fig. 7 High-resolution global cell atlas and unambiguous annotation of CNS myeloid cells.

(A) Integrated UMAP projection of 51,902 high-quality cells from all samples, annotated into 19 distinct cell types. (B) Canonical marker gene expression dot plot used for cell type annotation. Dot size represents the percentage of cells expressing the gene, and color intensity indicates average expression. Note the distinct separation between resident microglia (*Tmem119, P2ry12, Cx3cr1*) and infiltrating macrophages (*Ccr2, Ly6c2*), as well as CNS-resident lineages (*Olig1* for Oligodendrocytes, *Aqp4* for Astrocytes, *Map2* for Neurons).(C) Violin plots showing the expression of signature genes used to define the 8 microglial subpopulations described in Figure 6B.

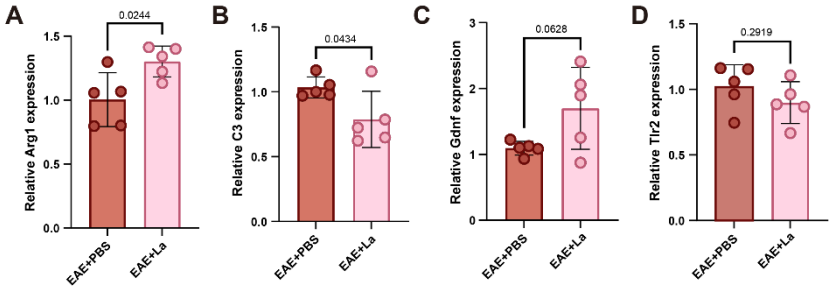

Fig. S8. RT-qPCR validation of key phenotypic genes in isolated microglia

(A-D) Relative mRNA expression levels of the reparative marker *Arg1* (A), the pro-inflammatory/DAM marker *C3* (B), the neurotrophic factor *Gdnf* (C), and the inflammatory receptor *Tlr2* (D) in pure microglia isolated from the CNS of PBS-treated (EAE+PBS) and lactate-treated (EAE+La) mice. Microglia were isolated using FACS sorting during the acute phase of EAE. Data are presented as mean ±SEM (n = 5 mice per group). Statistical significance was determined by an unpaired two-tailed Student's t-test. Source data are provided as a Source Data file.

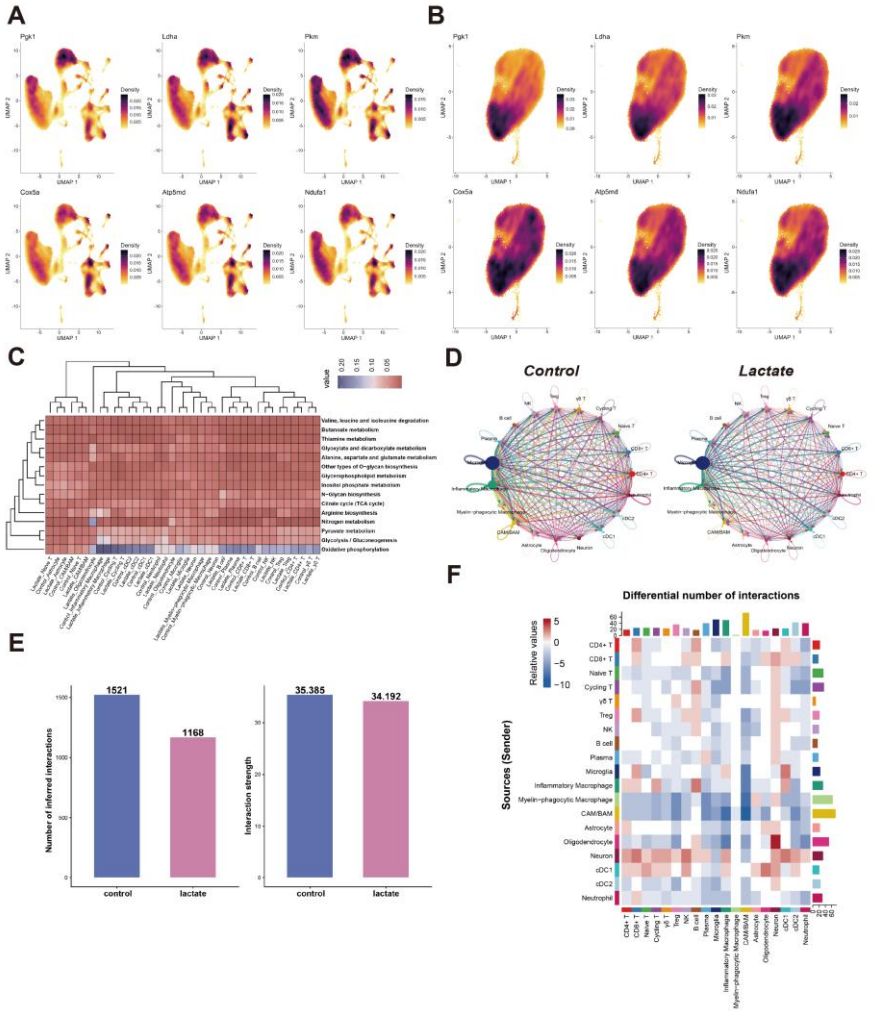

Supplementary Fig. 9 Metabolic gene expression landscapes and intercellular communication
(A-B) UMAP density plots illustrating the expression distributions of key genes involved in anaerobic glycolysis (*Pgk1, Ldha, Pkm*) and aerobic oxidative phosphorylation (*Cox5a, Atp5md, Ndufa1*). Panel (A) maps these genes across the global CNS cell atlas to show cell-type specificity, while Panel (B) focuses specifically on the microglial compartment to highlight metabolic heterogeneity across different activation states. Warmer colors indicate higher expression density.(C) Heatmap showing the enrichment scores of major metabolic pathways across all identified cell types.(D) Circle plots visualizing the inferred intercellular communication networks in Control (left) and Lactate (right) groups using CellChat. Lines represent ligand-receptor interactions.(E) Bar graphs quantifying the total number (left) and strength (right) of inferred interactions.(F) Heatmap of differential interaction strength. Red indicates signaling pathways increased in the Lactate group, while blue indicates pathways decreased compared to the Control group networks.

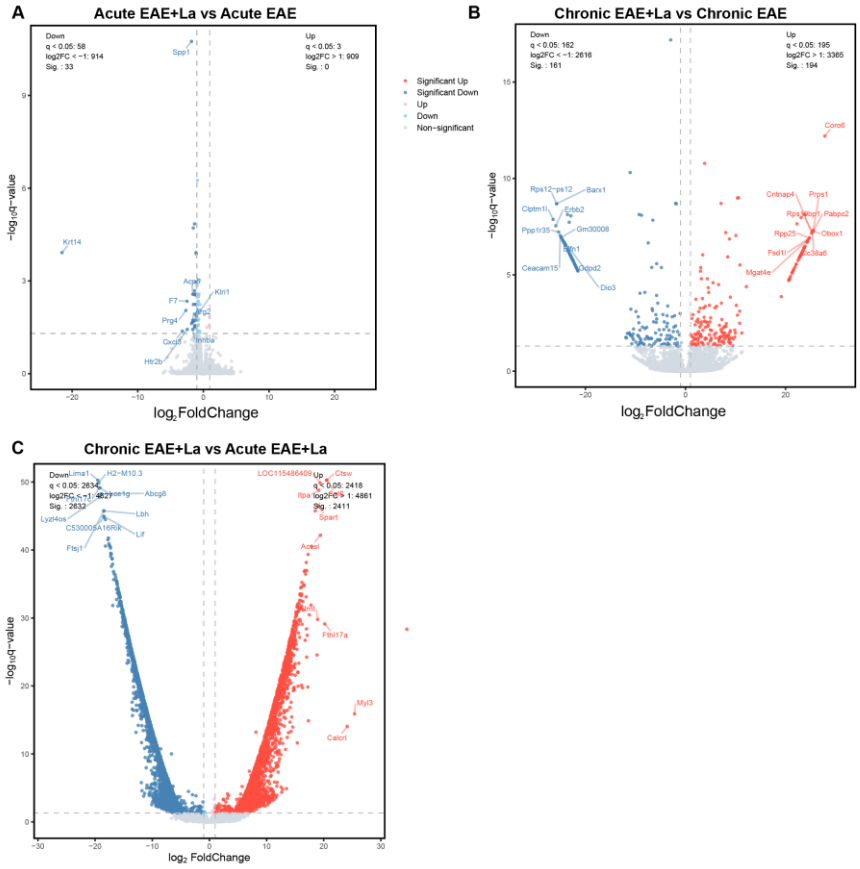

Supplementary Fig. 10 Global transcriptomic profiles of CNS myeloid cells under lactate treatment. (A-C) Volcano plots showing differentially expressed genes (DEGs) in isolated CD11b^{+} cells for the comparisons of Acute EAE+La versus Acute EAE (A), Chronic EAE+La versus Chronic EAE (B), and Chronic EAE+La versus Acute EAE+La (C). Red dots represent significantly upregulated genes, blue dots

represent significantly downregulated genes, and gray dots indicate non-significant genes.

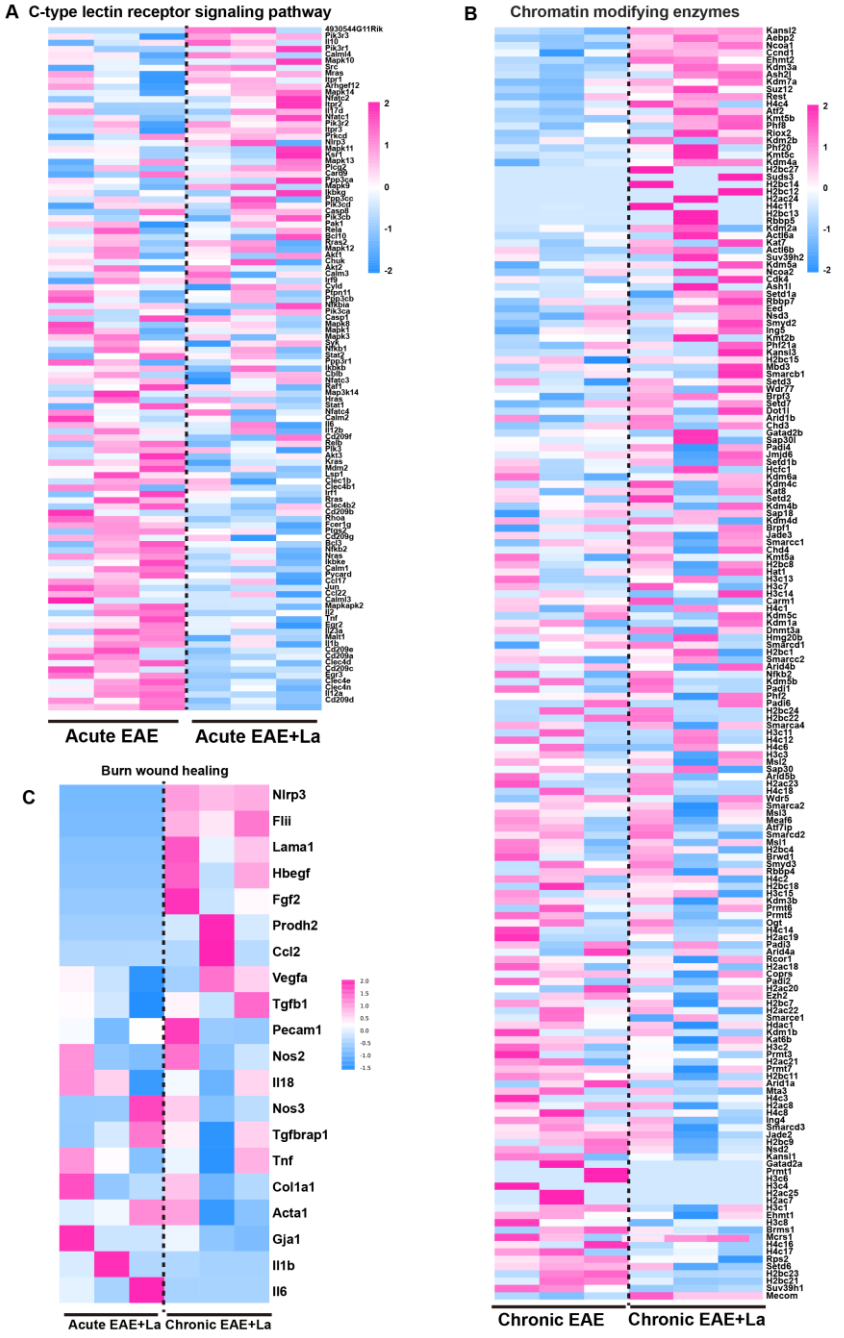

Supplementary Fig. 11 Detailed Gene Expression Heatmaps for Key Pathways Modulated by Lactate Treatment in EAE.

(A) Heatmap showing the expression of individual genes within the C-type lectin receptor signaling pathway" in microglia from Acute EAE and Acute EAE+La groups. (B) Heatmap showing the expression of individual genes within the "Chromatin modifying enzymes" gene set in microglia from Chronic EAE and Chronic EAE+La groups. (C) Heatmap showing the expression of individual genes within the "Burn wound healing" pathway, comparing microglia from the Chronic EAE+La group to the Acute EAE+La group to illustrate temporal evolution.

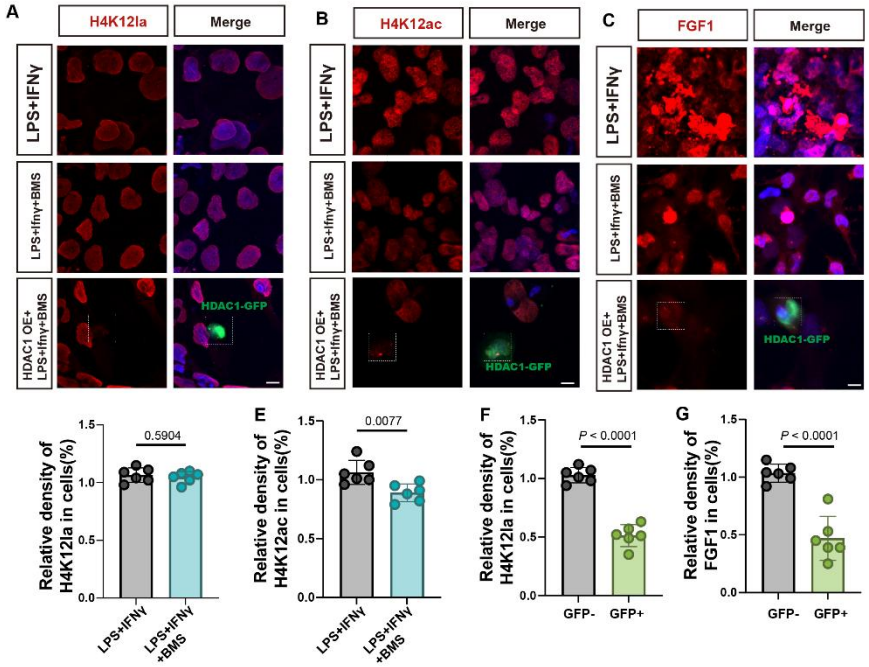

Supplementary Fig. 12 Verification of HDAC1-mediated delactylation.

(A-C) Representative immunofluorescence images for H4K12la (A), H4K12ac (B), and FGF1 (C) in red. HMC3 cells were stimulated with LPS+IFNγ alone or in combination with the ACLY inhibitor BMS-303141. The bottom row displays HDAC1-GFP (green) overexpression in cells pre-treated with BMS-303141. (D-E) Quantification of relative H4K12la (D) and H4K12ac (E) density following BMS treatment (n = 6 independent cell cultures). (F-G) Comparison of H4K12la (F) and FGF1 (G) signal density between GFP-negative and GFP-positive (HDAC1-overexpressing) nuclei (n = 6 independent cell cultures). Scale bars, 50 μm (applies to all image panels). Data represent mean ± SEM. Shapiro-Wilk tests were used to assess normality. Statistical significance was determined by an unpaired, two-tailed Student's t-test. Exact P values are indicated in the figure.

Supplementary Table 1. Patient demographics and disease characteristics

Patient ID	Diagnosis	Sex
P1	MS	F
P2	MS\AD	F
P3	MS	M
P4	MS	F
P5	MS	M
P6	MS	F
P7	MS	F
P8	MS	F
P9	MS	F
P10	MS	M
P11	MS	F
P12	MS	F
P13	MS	F
P14	MS	F
P15	MS	F
P16	MS	F
P17	MS	F
P18	MS	M
P19	MS	M
P20	MS	F

Supplementary Table 2. Laboratory parameters of individual patients

Patient ID	CSF OCB	CSF WBC ($\times10^6$/L)	CSF Lactate (mmol/L)	Blood WBC ($\times10^9$/L)	Neutrophil ($\times10^9$/L)	Lymphocyte ($\times10^9$/L)	IL-6 (pg/mL)	IL-10 (pg/mL)	CRP (mg/L)	EDSS Score
P1	Positive	4.0	1.5	8.1	5.38	2.03	3.07	1.18	2.0	0
P2	Weakly positive	2.0	2.0	5.34	4.33	0.45	5.29		2.0	6
P3	Weakly positive	2.0	1.6	12.55	9.17	2.11	2.29	3.04	4.0	7.5
P4	Negative	0.0	2.4	4.07	2.44	1.21	23.16	3.45	4.0	
P5	Weakly positive	9.0	2.0	7.08	4.33	2.14	2.83	1.83	1.0	2
P6	Negative	1.0	1.1	4.15	1.98	1.7	3.68	5.58	2.0	3.5
P7	Positive	4.0	1.5	7.89	6.96	0.71	4.34		2.0	2
P8	Weakly positive	0.0	1.0	10.55	6.5	3.28	2.11	2.22	2.0	3
P9	Positive	8.0	1.1	10.44	9.07	0.96	8.84	5.62	1.0	2
P10	Positive	7.0	1.3	8.84	5.17	2.95			2.0	2
P11	Positive	6.0	1.6	3.83	1.69	1.75	1.5		1.0	3.5

P12	Positive	1.0	1.6	4.52	2.39	1.81	1.95		1.0	8
P13	Negative	1.0	1.4	4.71	2.52	1.68	2.82		2.0	2
P14	Negative	0.0	1.6	5.62	3.3	1.87	4.7	2.57	1.0	
P15	Positive	2.0	1.7	10.99	9.88	0.68	2.12	1.31		6
P16	Positive	7.0	1.2	7.24	4.58	2.27	5.89		5.0	2
P17	Negative	3.0	1.3	5.96	3.6	1.96			1.0	0
P18	Negative	23.0	1.6	5.77	4.83	0.43	7.82		5.0	3.5
P19	Positive	3.0	1.1	7.05	6.91	0.90	4.02		2.0	
P20	Negative	1.0	1.6	10.59	8.73	1.6	1.08	1.96	2.0	

Supplementary Table 3 Detailed information of the control subjects included in the study

Patient ID	Clinical presentation	Sex	CSF Lactate (mmol/L)
P21	Dizziness	M	1.4
P22	Lower limb weakness	M	1.4
P23	Hemiparesis	M	1.2
P24	Headache, Central atrial septal defect	M	1.3
P25	Ataxia	F	1.4
P26	Dizziness, Nystagmus	M	1.6
P27	Intracranial hypertension syndrome	F	1.2
P28	Psycho-behavioral disorder	M	1.3
P29	Cognitive impairment	F	1.3
P30	Ataxia	F	1.4
P31	Internal jugular vein stenosis	M	1.3
P32	Cranial venous sinus thrombosis	M	1.3
P33	Ataxia	F	1.5
P34	Epilepsy	F	1.2
P35	Psycho-behavioral disorder	M	1.2
P36	Internal jugular vein stenosis	F	1.4
P37	Intracranial hypertension syndrome	M	1.4
P38	Internal jugular vein stenosis	F	1.5

P39	Ataxia	M	1.2
P40	Vitamin B12 deficiency, Ataxia	M	1.6

Supplementary Table 4 List of PCR primers

Gene	Forward	Reverse
FGF1 (Human)	CTCCCGAAGGATTAAACGACG	GTCAGTGCTGCCTGAATGCT
GDNF (Human)	GGCAGTGCTTCCTAGAAGAGA	AAGACACAACCCCGGTTTTTG
ACTIN (Human)	CCTGGACTTCGAGCAAGAGATGG	CAGGAAGGAAGGCTGGAAGAGTG
LDHA (Human)	TTTCACACACACACCCCCAA	TGCTTAGCATGAGACCGTGC
C3(Mouse)	AGCAGGTCATCAAGTCAGGC	GATGTAGCTGGTGTTGGGCT
Arg1 (Mouse)	CTCCAAGCCAAAGTCCTTAGAG	AGGAGCTGTCATTAGGGACATC
Tlr2(Mouse)	GCAAACGCTGTTCTGCTCAG	AGGCGTCTCCCTCTATTGTATT
Gdnf (Mouse)	GATTCGGGCCACTTGGAGTT	GACAGCCACGACATCCCATA
Actin (Mouse)	GGCTGTATTCCCCTCCATCG	CCAGTTGGTAACAATGCCATGT

Supplementary Table 5 Antibodies used in this study

Antibodies	Source	Identifier
Rabbit polyclonal anti-Pan Kla	PTM BIO	Cat# PTM-1401
Rabbit polyclonal anti-H4K12la	PTM BIO	Cat# PTM-1411
Rabbit monoclonal anti-H3K18la	PTM BIO	Cat# PTM-1406RM
Rabbit monoclonal anti-H3K9la	PTM BIO	Cat# PTM-1419RM
Rabbit monoclonal anti-H3K14la	PTM BIO	Cat# PTM-1414RM
Anti-Histone H3 Rabbit mAb	PTM BIO	Cat# PTM-1001RM
Anti-Histone H4 Rabbit mAb	PTM BIO	Cat# PTM-1015RM
Rabbit polyclonal anti-Iba1	Abcam	Cat# ab178847,
Guinea pig anti-Iba1	Oasisbiofarm	Cat#OB-PGP049
Mouse polyclonal anti-NeuN	Abcam	Cat# ab104224
Rat polyclonal anti-GFAP	invitrogen	Cat# 13-0300
Mouse polyclonal anti-Arg1	Santa Cruz Biotechnology	Cat# sc-271430
Mouse polyclonal anti-NOS2	Santa Cruz Biotechnology	Cat# sc-7271

Rabbit polyclonal anti-HK2	Huabio	Cat# ER1803-23
Rabbit polyclonal anti-LDHA	Huabio	Cat# ER00702
Rabbit polyclonal anti-GDNF	Huabio	Cat# ET1704-46
Rabbit polyclonal anti-FGF1	Huabio	Cat #HA722695
Rabbit polyclonal anti-HDAC1	Huabio	Cat# ET1605-35
Mouse polyclonal anti-HDAC1	Proteintech	Cat#No. 66085-1-Ig
Mouse Anti-β actin mAb	ZSGB-Bio	Cat# TA-09
Mouse Anti-β tubulin mAb	ZSGB-Bio	Cat# TA-10
Donkey anti-Rabbit IgG (H+L) Highly Cross-Adsorbed Secondary Antibody, Alexa Fluor™ 488	Thermo Fisher Scientific	Cat# A-21206
Donkey anti-Mouse IgG (H+L) Highly Cross-Adsorbed Secondary Antibody, Alexa Fluor™ 546	Thermo Fisher Scientific	Cat# A10036
Donkey anti-Rat IgG (H+L) Highly Cross-Adsorbed Secondary Antibody, Alexa Fluor™ 647	Thermo Fisher Scientific	Cat# A78947
Horseradish enzyme labeled goat anti-rabbit IgG (H+L)	ZSGB-Bio	Cat# ZB-2301
Horseradish enzyme labeled goat anti-mouse IgG (H+L)	ZSGB-Bio	Cat# ZB-2305
PE anti-mouse CD45	BioLegend	Cat# 103106
Brilliant Violet 650(TM) anti-mouse CD4	BioLegend	Cat# 100546
APC anti-mouse CD8a	BioLegend	Cat# 100712
Brilliant Violet 711(TM) anti-mouse/human CD11b	BioLegend	Cat# 101242

Supplementary Table 6 Key reagents and commercial assays

Reagent or Resource	Source	Identifier
Tamoxifen	Solarbio	Cat# T9010
Corn oil	Beyotime	Cat# ST2306
MOG33-35	Genscript	Cat# SC1208
PTX	List labs	Cat# 181
TB	BD	Cat# 231141
CFA	Sigma-Aldrich	Cat# F5881
LPS	Sigma-Aldrich	Cat# L2880
IFN-γ	MCE	Cat# HY-P7025
MS-275	MCE	Cat#HY-12163
BMS-303141	Selleck	S0277

anti-CD11b-coated MicroBeads	Miltenyi Biotec	Cat# 130-093-634
Hyperactive Universal CUT&Tag Assay Kit for Illumina Pro	Vazyme Biotech	Cat# TD904-01
VAHTS DNA Clean Beads	Vazyme Biotech	Cat# N411
CheKine™ Micro Lactate Assay Kit	Abbkine	Cat# KTB1100
Enhanced BCA Protein Assay Kit	Beyotime	Cat# P0010
Lip2000 Transfection Reagent	Biosharp	Cat# BL623A
FastKing One Step RT-PCR Kit	TIANGEN	Cat# KR123